Applied Catalysis A: General 470 (2014) 56–62

Contents lists available at ScienceDirect

Applied Catalysis A: General

journal homepage: www.elsevier.com/locate/apcata

A facile and eco-friendly synthesis of imidazo[1,2-*a*]pyridines using nano-sized $LaMnO_3$ perovskite-type oxide as an efficient catalyst under solvent-free conditions

Tayebeh Sanaeishoar[a], Haman Tavakkoli[a,*], Fouad Mohave[b]

[a] Department of Chemistry, Science and Research Branch, Islamic Azad University, Khouzestan, Iran
[b] Young Researchers Club, Khouzestan Science and Research Branch, Islamic Azad University, Ahvaz, Iran

ARTICLE INFO

Article history:
Received 19 June 2013
Received in revised form 12 October 2013
Accepted 16 October 2013
Available online xxx

Keywords:
Perovskite-type oxide
Nanoparticles
Reusable heterogeneous catalyst
Three-component reactions
Solvent-free

ABSTRACT

$LaMnO_3$ perovskite nanoparticles were prepared using a sol–gel method. The physical and chemical properties of the catalyst were determined using X-ray diffraction, transmission electron microscopy, scanning electron microscopy, Energy dispersive X-ray spectroscopy, BET method and Fourier transform infrared spectroscopy. The XRD results indicated that the $LaMnO_3$ has a good crystalline phase at 600 °C. The BET surface area of the mesoporous perovskite materials ($LaMnO_3$) was 475 m^2/g and the average width of the pores was 8.7 nm. The experimental data revealed that the $LaMnO_3$ particles were nano-sized. This perovskite-type oxide as a green and reusable catalyst showed excellent catalytic activity for the synthesis of imidazo[1,2-*a*]pyridines. $LaMnO_3$ catalyst could be recovered and reused in five reaction cycles, giving a total TON = 2790 and TOF = 372. The products were prepared under solvent-free conditions without any additives. Principal features of this simple method include non-hazardous reaction conditions, low catalyst loading and excellent yields.

1. Introduction

Nitrogen-containing heterocycles are abundant in nature and exhibit diverse and important biological properties [1–4]. Among them, imidazo[1,2-*a*]pyridine derivatives display a diverse range of biological activities such as antimicrobial [5], inhibitors of HIV-1 reverse transcriptase [6], biological activity against colon cancer [7], potent inhibitor of p38 MAP kinase [8], inhibitor of cyclin dependent kinases [9] and treatment of anxiety disorders [10]. A new three-component condensation to approach such fused imidazoles was developed simultaneously by Groebke, Bienayme, and Blackburn in 1998 [11–13]. Since the first reports were published, various methods have been performed to improve this powerful MCR (multi component reaction) synthetic methodology. Some of these methods used acidic catalysts [14–16], some supported acid catalysts [17–19], in the presence of polar solvents [20–22], ionic liquids [23] and under catalyst-free [24], neat condition [25,26], and microwave irradiation [27,28]. However, these methods possess several disadvantages such as long reaction time [11–13,24,25], complicated work-up procedure and harsh reaction conditions [17,27], requirement of excess amount of catalysts [11,12,14], and low yields [27,29].

A wide cross-fertilization bridges heterogeneous catalysis and materials science in the areas of physicochemical characterization, solid-state chemistry, and synthetic routes [30–32]. Among mixed metal oxides, perovskite-type oxides are prominent. Perovskite-type mixed metal oxides of chemical formula ABO_3 (A is a larger cation than B) have attracted interest over the years owing to their unique physical and chemical properties [33]. Perovskites have many possible applications, e.g., in electrical devices [34], as ferromagnetic material [35], in membranes for gas separation [36], as catalysts [37,38], as promising adsorbents [39,40] and in sensors [41], and the catalytic properties are important in most applications.

Perovskites also efficiently catalyse organic reactions at very low catalyst loadings [42–45]. The small amount of precious or active metal oxides in the perovskite implies very high turnover numbers. Furthermore the catalysts are readily removed by filtration, are recyclable and lead to extremely low leaching into solution making perovskites an attractive alternative to homogeneous catalysis. An important feature of $LaMnO_3$ and many related perovskites is their ability to reversibly adsorb and desorb oxygen into the crystal lattice by continuous and spontaneous changes in Mn oxidation state, without changing the overall bulk crystal structure [46]. Therefore, the present study has investigated fabrication and characterization of perovskite-type oxide nanoparticles $LaMnO_3$ and determination its efficiency as a promising nanocatalyst for synthesis of imidazo[1,2-*a*] pyridine derivatives using very low amount

* Corresponding author. Tel.: +98 611 4457612; fax: +98 611 4435288.
E-mail address: h.tavakkoli@khouzestan.srbiau.ac.ir (H. Tavakkoli).

0926-860X/$ – see front matter © 2013 Published by Elsevier B.V.
http://dx.doi.org/10.1016/j.apcata.2013.10.026

of sufficient recyclable catalyst and eliminate the use of auxiliary substances e.g. solvents, separation agents, etc.

2. Experimental

2.1. General remarks

All chemicals and reagents were obtained from Sigma–Aldrich or Merck and were used without further purification. Several techniques were employed to analyze and validate the synthesized nanocatalyst. For structural investigation of calcined powder at 650 °C X-ray diffraction (XRD) measurements were carried out in the region of ($2\theta = 20^\circ$ to 70°) using Cu$K\alpha$ radiation on a Rigaku D/MAX RB XRD diffractometer equipped with a curved graphite monochromator. The microstructure of powder was examined using LEO 912AB TEM under a working voltage of 120 kV, while the morphology and chemical analysis of the particles was investigated using SEM–EDX technique. The SEM of the type LEO 1450 VP ($V = 30$ kV) was equipped with an EDX spectrometer of the type Inca 400 (Oxford Instruments). The melting points of products were determined with an Electrothermal 9200 melting point apparatus. The FT-IR spectra were recorded on a Perkin-Elmer BX-II IR spectrometer. The ^{1}H NMR and ^{13}C NMR spectra were provided on Bruker DRX-400 and DRX-300 Avance instruments in $CDCl_3$. The specific surface area (SSA) of the catalyst was calculated using BET method from the nitrogen adsorption isotherms obtained at 77 K on samples outgassed at 250 °C with the use of a Micromeritics Accusorb 2100E apparatus.

2.2. Preparation of catalyst ($LaMnO_3$)

$LaMnO_3$ (LMO) of the type perovskite oxide were fabricated by sol–gel method. The appropriate amounts of starting materials $La(NO_3)_3{\cdot}6H_2O$ (99.9%) and $Mn(CH_3COO)_2{\cdot}H_2O$ (99.9%) were dissolved in deionized water. Citric acid was then added slowly to the metal solution at room temperature under constant magnetic stirring (1000 r/min). The solution was refluxed with stirring for 2 h to convert it to a stable complex. To make a gel, stirring was continued at ~70 °C for 3 h in water bath. A dry gel was obtained by placing the sol in an oven and heating slowly to 110 °C and then maintaining the temperature for 8 h. The gel was ground in an agate mortar to give a powder. $LaMnO_3$ nanoparticles were obtained by calcinations of the precursors at 650 °C for 9 h in air.

2.3. Preparation of catalyst ($FeCl_3{\cdot}$nano-SiO_2)

The $FeCl_3{\cdot}$nano-SiO_2 was prepared by reported method [47]. In a 100 mL flask, nano silica gel (25 g) and $FeCl_3{\cdot}6H_2O$ (2 g) (8% of the weight of nano-SiO_2) were vigorously stirred by magnetic stirrer under solvent-free conditions at room temperature for 24 h to achieve a homogeneous adsorption. A yellow powder was obtained. This powder was heated for 1 h at 100 °C to give a brownish powder ("active" $FeCl_3$/nano-$SiO_2{\cdot}$reagent).

2.4. Preparation of catalyst ($FeCl_3{\cdot}Al_2O_3$)

The $FeCl_3{\cdot}Al_2O_3$ was prepared by reported method [48], by mixing with ~10% its weightof iron chloride hexahydrate ($FeCl_3{\cdot}6H_2O$) 8 g in acetone (72 mL) and adding 43.2 g neutral Al_2O_3. The mixture was stirred at room temperature for 1 h. The acetone was removed under reduced pressure. The resulting yellow-brown powder was dried at 120 °C for 4 h.

2.5. Preparation of catalyst (KF·γ-Al_2O_3)

The KF·γ-Al_2O_3 was prepared by reported method [49]. Supported KF on γ-alumina with loadings of 3–15 mmol KF/g was prepared by the wet impregnation method. γ-Alumina was added to a solution of KF in water and the suspension was stirred at room temperature for 2 h. Water as evaporated at 60 °C under reduced pressure using a rotary evaporator. The catalyst was dried at 100 °C overnight, and pretreated in vacuum at the desired temperature before testing for any catalytic activity.

2.6. Preparation of catalyst ($NH_4OAc{\cdot}Al_2O_3$)

Alumina (ICN Biomedical *N*-Super 1, 9.23 g) was added to a solution of ammonium acetate (10 mmol, 0.77 g) in methanol, and the mixture was stirred at room temperature for 0.5 h. The methanol was removed by rotary evaporator under reduced pressure, and the resulting reagent was dried in vacuum (10 mmHg) at room temperature for 2 h [50].

2.7. Typical procedure for the synthesis of imidazo[1,2-a]pyridines

To a mixture of aldehyde(1 mmol), amidine(1 mmol) and isocyanide(1 mmol), nano-$LaMnO_3$ (0.0005 g) was added and the mixture was heated at 35 °C for an appropriate time as indicated by TLC. The mixture was filtered and washed with CH_2Cl_2 to separate catalyst. To obtain pure products the solid residue was recrystallized from CH_3CN.

All the products (except of **4a**, **4b**, **4c**, **4f** and **4 h**) are new compounds, which were identified by IR, ^{1}H NMR and ^{13}C NMR spectral data.

2.8. Spectral data of synthesized imidazo[1,2-a]pyridines

2.8.1. N-Cyclohexyl-2-(4-(dimethylamino)phenyl)imidazo[1,2-a]pyridin-3-amine (**4d**, $C_{21}H_{26}N_4$)

Yellow-brown crystal, (0.314 g, 94%); mp: 182–183 °C; IR (KBr, cm^{-1}): 3432(NH), 2926 (CH), 1630 and 1462 (Ar). ^{1}H NMR ($CDCl_3$, 400 MHz): $\delta = 1.17$–1.86 (10*H*, m, 5 CH_2 of CyHex), 3.02 (1 *H*, m, CHN of CyHex), 3.02 (6*H*, s, 2CH_3), 3.27 (1*H*, s, NH), 6.81 (3*H*, m, 3 CH of Ar), 7.15 (1*H*, dd, J, ^{3}J = 8.4, ^{4}J = 7.2, CH of Ar), 7.62 (1*H*, d, ^{3}J = 8.8, CH of Ar), 7.98 (2*H*, d, ^{3}J = 6.8, 2 CH of Ar), 8.15 (1*H*, d, ^{3}J = 6.8, CH of Ar). ^{13}C NMR ($CDCl_3$, 100 MHz): $\delta = 24.86, 25.81, 34.15, 40.47, 56.80, 111.14, 112.32, 116.77, 122.54, 122.58, 123.36, 123.55, 127.84, 137.10, 141.36, 149.67$.

2.8.2. N-Cyclohexyl-2-(9H-fluoren-2-yl)imidazo[1,2-a]pyridin-3-amine (**4e**, $C_{26}H_{25}N_3$)

Yellow-brown crystal, (0.360 g, 95%); mp: 172–174 °C; IR (KBr, cm^{-1}): 3222 (NH), 2926 (CH), 1638 and 1444 (Ar). ^{1}H NMR ($CDCl_3$, 400 MHz): $\delta = 1.18$–1.87 (10*H*, m, 5 CH_2 of CyHex), 3.01 (1 *H*, m, CHN of CyHex), 3.63 (1*H*, s, NH), 4.00 (2*H*, s, CH_2), 6.79 (1 *H*, td, ^{3}J = 6.8, ^{4}J = 0.8, CH of Ar), 7.16 (1 *H*, m, CH of Ar), 7.34 (1 *H*, td, ^{3}J = 7.6, ^{4}J = 1.2, CH of Ar), 7.39 (1 *H*, m, CH of Ar), 7.58 (1 *H*, d, ^{3}J = 7.2, CH of Ar), 7.65 (1 *H*, d, ^{3}J = 8.8, CH of Ar),), 7.81 (2 *H*, m, 2 CH of Ar), 8.10 (1 *H*, dd, ^{3}J = 7.8, ^{4}J = 1.4, CH of Ar), 8.19 (1 *H*, d, ^{3}J = 6.8, CH of Ar), 8.33 (1 *H*, d, ^{3}J = 0.4, CH of Ar). ^{13}C NMR ($CDCl_3$, 100 MHz): $\delta = 24.83, 25.76, 34.21, 37.04, 56.87, 111.51, 117.13, 119.82, 119.92, 122.72, 123.79, 123.94, 124.94, 125.07, 125.55, 126.66, 126.79, 133.01, 136.81, 140.78, 141.51, 141.62, 143.64, 143.66$.

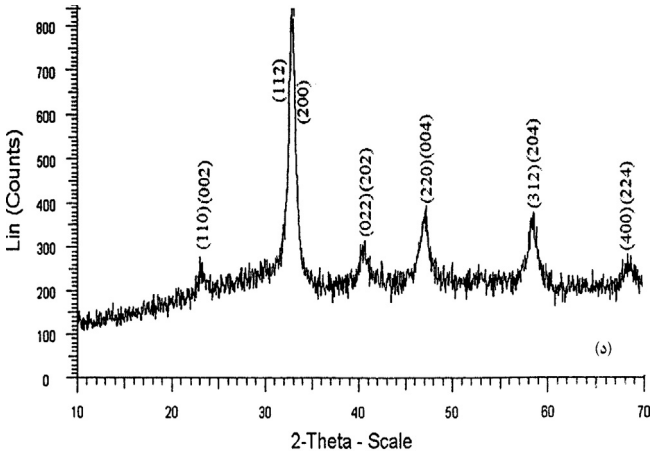

Fig. 1. XRD patterns of samples of the LMO nanopowder calcinated at 650 °C.

*2.8.3. 2-(4-Chlorophenyl)-N-cyclohexyl-7-methylimidazo[1,2-a]pyridin-3-amine (**4l**, $C_{20}H_{22}ClN_3$)*

White crystals, (0.333 g, 98%); mp: 208–209 °C; IR (KBr, cm^{-1}): 3235 (NH), 2922 (CH), 1644 and 1467 (Ar). ^{1}H NMR ($CDCl_3$, 400 MHz): δ = 1.17–1.82 (10 *H*, m, 5 CH_2 of CyHex), 2.44 (3*H*, s, CH_3), 2.93(1 *H*, m, CHN of CyHex), 3.86 (1*H*, br s, NH), 6.79 (1 *H*, d, ^{3}J = 6.8, CH of Ar), 7.37 (2 *H*, m, CH of Ar), 7.48 (1 *H*, s, CH of Ar), 8.08 (3 *H*, m, CH of Ar). ^{13}C NMR ($CDCl_3$, 100 MHz): δ = 21.36, 24.81, 25.71, 34.16, 56.90, 114.54, 115.59, 122.02, 124.48, 128.16, 128.60, 132.82, 132.89, 134.89, 135.46, 141.93.

3. Results and discussion

3.1. Characterization of the catalyst

The nanopowders of perovskite-type oxides $LaMnO_3$ were fabricated by sol–gel method in the presence of citric acid as a chelating agent. The obtained nanoparticles were characterized by XRD, TEM, SEM, BET and EDX methods.

3.1.1. X-ray diffraction studies

Fig. 1 shows the XRD patterns of the $LaMnO_3$ nanoparticles prepared by sol–gel method and calcined at 650 °C for 9 h. The diffractograms reveal that the crystalline perovskite structure is the main phase for synthesized powders. The diffraction peaks at 2θ angels appeared in the order of 23°, 32.5°, 41°, 47°, 58.5° and 68.65° and they can be assigned to scattering from the (1 1 0), (1 1 2), (0 2 2), (2 2 0), (3 1 2) and (4 0 0) planes of the $LaMnO_3$ perovskite type crystal lattice, respectively. XRD data shows $LaMnO_3$ crystallized in rhombohedral system [51]. No additional peak is seen in the XRD pattern of the catalyst which reveals the high purity of the prepared perovskite nanoparticles. The average crystallite size can be calculated using the XRD peak broadening of the (2θ = 32.5°) peak by the well known Scherer's formula:

$$D_{hkl} = \frac{0.9\lambda}{\beta_{hkl} \cos \theta_{hkl}} \quad (1)$$

where D_{hkl} (nm) is the particle size perpendicular to the normal line of (*hkl*) plane, β_{hkl} is the full width at half maximum, θ_{hkl} (Rad) is the Bragg angle of (*hkl*) peak, and λ (nm) is the wavelength of X-ray. The crystallite size of $LaMnO_3$ calcinated at 650 °C was about 28 nm.

3.1.2. Morphology, pore structure and surface area

The morphology and the particle size of $LaMnO_3$ nanoparticles were studied by TEM and SEM methods. The TEM image of these nanopowders is shown in Fig. 2. All the particles display the uniform quasi-spherical morphology with the average particle size of about 25 nm, which is in a good agreement with the results achieved from XRD measurement.

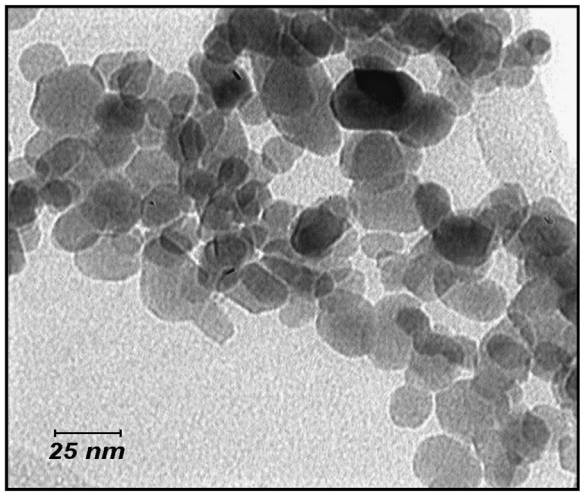

Fig. 2. TEM image of the LMO nanoparticles.

Scanning electron microscopy (SEM) of perovskite oxide prepared by the sol–gel method and calcined at 650 °C is shown in Fig. 3. Based on the SEM images, porosity of the surface is evident and it seems that the particles have grown with uniform size. The particles size that was propagated on the surface seems to be in the range of 25–100 nm.

In addition, energy-dispersive X-ray (EDX), as shown in Fig. 4, confirmed the existence of La, Mn and O ratio as well as the phase-purity of the nanopowders.

The specific surface area of the catalyst was measured by means of conventional BET method (Fig. 5). Results showed that the average of specific surface area of LMO nanoparticle was 475 m^2/g. Mesopore volume and mesopore width were obtained from DR method are 0.27 cm^3/g and 8.7 nm, respectively. According to IUPAC classification, N_2 adsorption–desorption isotherm of nanoparticles LMO is type IV. This isotherm is the characteristic of adsorption–desorption on mesoporous solids. So, it seems that the large specific surface area of the catalyst is an advantage for the synthesis of imidazo[1,2-*a*] pyridine derivatives.

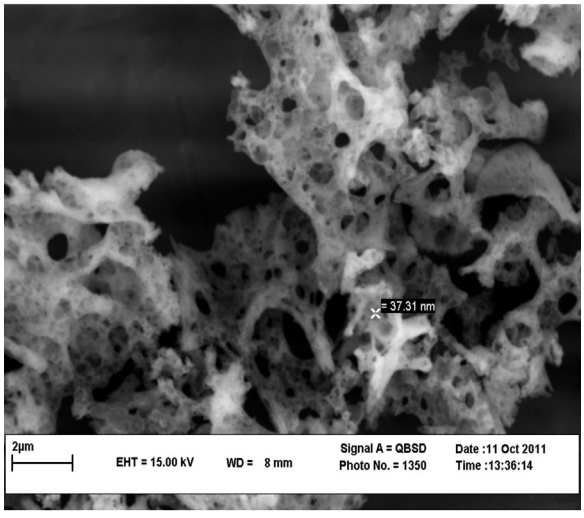

Fig. 3. SEM images of LMO nanopowders.

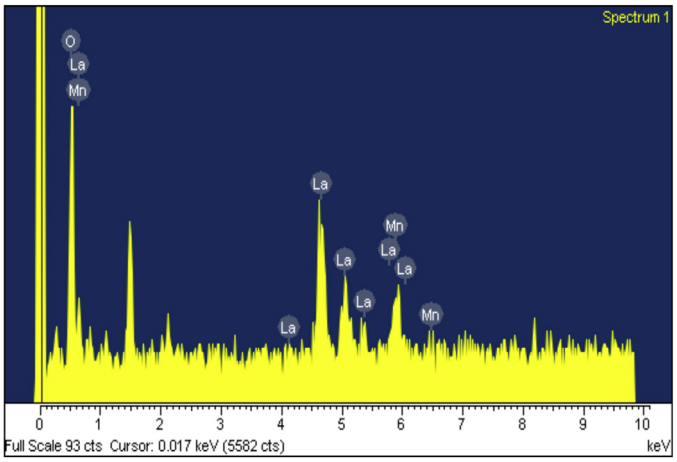

Fig. 4. Energy dispersive X-ray (EDX) spectrum of the LMO nanoparticles.

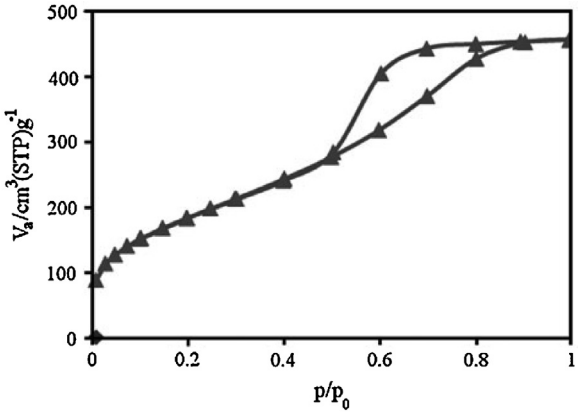

Fig. 5. N_2 adsorption–desorption isotherm of LMO is calcinated at 650 °C.

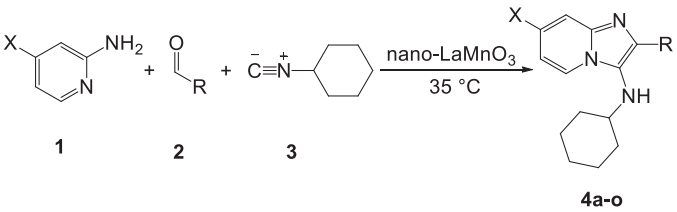

Scheme 1. Synthesis of compounds **4a–4o**.

3.2. Catalytic application of $LaMnO_3$ nanoparticles in synthesis of imidazo[1,2-a] pyridine derivatives

To explore the catalytic activity of this heterogeneous catalyst, we investigated its efficiency in the reaction between 2-aminopyridine, benzaldehyde, and cyclohexyl isocyanide under solvent-free conditions within 1.5 h at 35 °C (Scheme 1). In order to optimize the reaction conditions, we conducted this reaction with various solvent systems; it was observed that solvent-free condition gave the best result in terms of reaction time and yield (Table 1).

3.2.1. Catalyst loading

The required quantity of catalyst was probed by performing the condensation reaction of 2-aminopyridine, benzaldehyde and cyclohexyl isocyanide at six different nano-$LaMnO_3$ loadings.

Table 1
Initial solvent effect studies for synthesis of 3-aminoimidazo[1,2-*a*]pyridines with 0.2 mol% catalyst.

Entry	Solvent	Temp (°C)	Time (h)	Yield (%)
1	CH_2Cl_2	Reflux	24	35
2	CH_3CN	Reflux	24	<30
3	EtOH	Reflux	24	55
4	MeOH	Reflux	24	55
5	Acetone	Reflux	24	<30
6	H_2O	Reflux	24	<30
7	Toluene	Reflux	24	50
8	*n*-Hexane	Reflux	24	50
9	Ethyl acetate	Reflux	24	45
10	**Solvent-free**	**35**	**1.5**	**96**

Conditions: aminopyridine (1 mmol), benzaldehyde (1 mmol), cyclohexyl isocyanide (1 mmol) and 0.2 mol% nano-$LaMnO_3$ in 2 mL solvent, stirring.

Effective catalysis was demonstrated down to 0.2 mol% (0.0005 g) of nano-$LaMnO_3$ (Table 2). We observed that taking reaction in the room temperature gave low yields of the desired products (entry 10). The yield increased sharply when the temperature was raised from room temperature to 35 °C. A further increase in the amount of catalyst (up to 10 mol%) and of the reaction temperature did not have any significant effects on the product yield or reaction time. It should be noted that in the absence of catalyst a very low amount of the desired product was formed (entry 1). However other catalysts such as $FeCl_3$·nano-SiO_2, $FeCl_3$·Al_2O_3, KF·γ-Al_2O_3 and NH_4OAc·Al_2O_3 were examined, which afforded relatively low yield of compounds and higher catalyst loading. In general Bronsted or Lewis acids as well as solid acids promoters give the best results in terms of yield and reaction time. Moreover, the use of $FeCl_3$·nano-SiO_2, $FeCl_3$·Al_2O_3 and $LaMnO_3$ as Lewis acid catalysts afforded the higher yield comparing to basic catalysts. High activity of the $LaMnO_3$ along with Lewis acidic center depends on the high surface area and the perovskite structure, these attributes playing a very important role to synthesis desired products, also these features are the main reasons for $LaMnO_3$ to obtain higher yields comparing to other catalyst (Table 2). In order to show the effectiveness of the present work with respect to the previous reports, nano-$LaMnO_3$ was compared with mentioned examples as well (see entries 7–10).

3.2.2. Catalytic performance

After optimizing the conditions, to explore the scope and limitations of this reaction we studied the reactions of 2-aminopyridine or 4-methyl-2-aminopyridine **1** and isocyanide **3** with various aromatic aldehydes **2** all desired products were formed as shown in (Table 3). As expected, we have found that the reactions of electron-withdrawing aldehydes have higher yields compared to the reactions of electron donating aldehydes. Despite the expectations, reactions of 4-methyl-2-aminopyridine have lower yields comparing to 2-aminopyridine.

3.2.3. Reusability of catalyst

To evaluate the stability of catalytic activity and the potential for recycling, we completed several catalytic cycles. When the reaction was completed, the catalyst was separated by filtration. Then the catalyst was washed with CH_2Cl_2 (3 × 5 mL) and subsequently dried at 50 °C to the reused. As shown in Fig. 6 nano-$LaMnO_3$ could be reused in subsequent reactions without any decrease in catalytic activity even after five runs. Turn over number (TON) and turn over frequency (TOF) of **4a** after the fifth run were calculated, TON = 2790 and TOF = 372 h^{-1} and compared to the previous report TON = 453 and TOF = 82.4 h^{-1} [26].

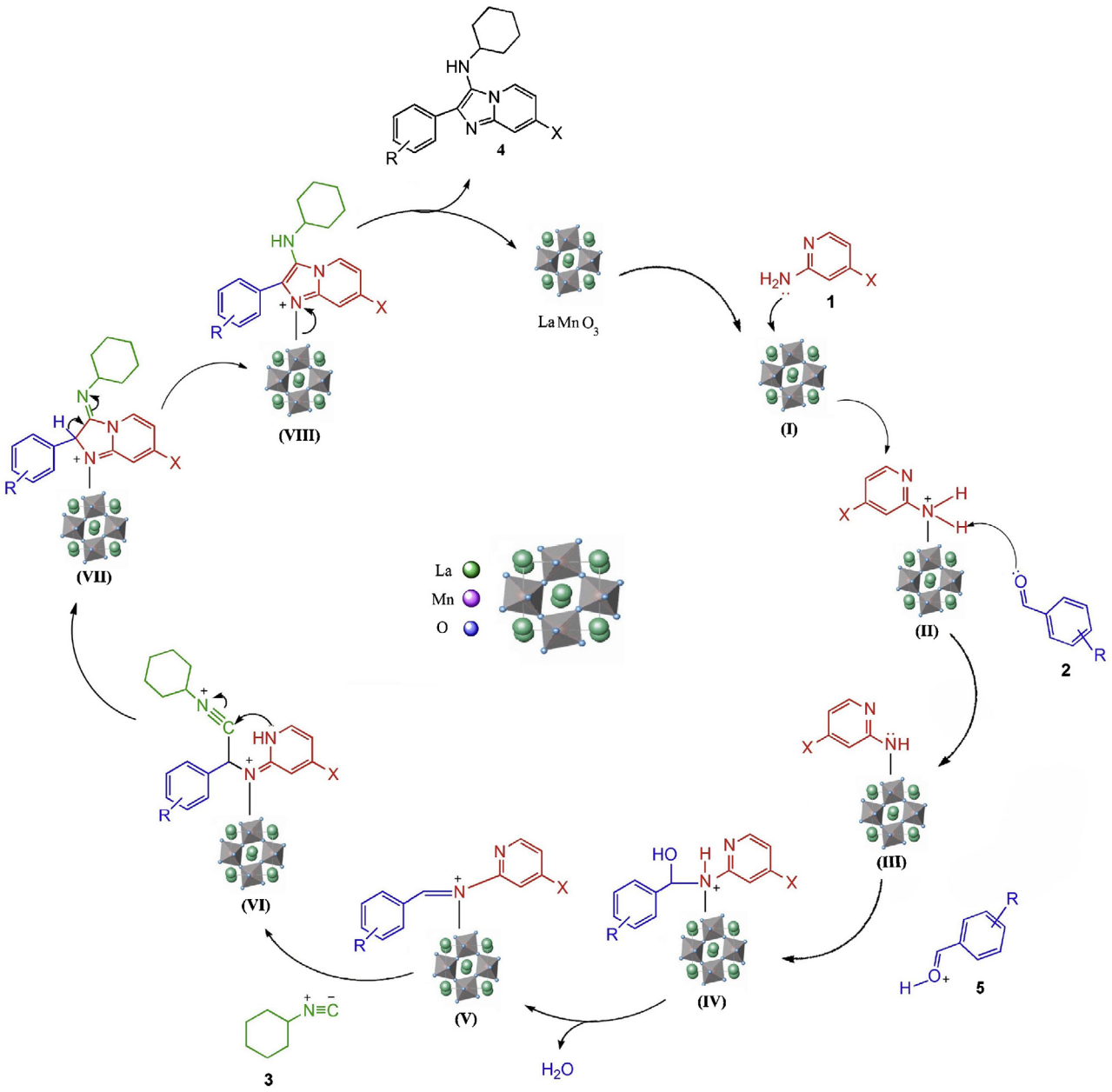

Scheme 2. A plausible mechanism using nano-$LaMnO_3$.

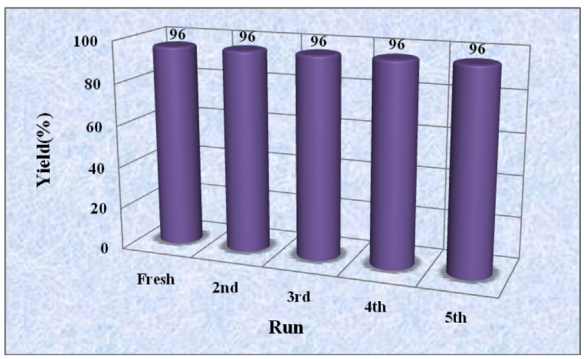

Fig. 6. Yield refers to isolated products from the aminopyridines (1 mmol), benzaldehyde (1 mmol), cyclohexylisocyanide (1 mmol) in the presence of 0.2 mol% nano-$LaMnO_3$ (0.0005 g) under solvent-free condition.

3.2.4. *A plausible mechanism for synthesis of imidazo[1,2-a]pyridine using $LaMnO_3$*

On the basis of the experimental observations and previously reported mechanism [11–13], the possible pathway for the formation of imidazo[1,2-*a*]pyridine over $LaMnO_3$ nanoparticles can be explained as follows (Scheme 2): Initially, 2-aminopyridine **1** coordinates to the Lewis acidic site present at the catalyst surface (**I**). The protonation of **2** by the NH-acidic of compound (**II**) and the subsequent attack of the resulting nucleophile (**III**) on the activated carbonyl of aldehyde **5** afforded (**IV**). The elimination of the water leads to iminium salt (**V**), then it undergoes nucleophilic addition with the isocyanide **3** to form the isonitrilium intermediate (**VI**), which cyclizes into the imino intermediate (**VII**). This intermediate tautomerizes under the reaction conditions to afford the 3-alkylamino-2-arylimidazo[1,2-*a*]pyridine (**VIII**), The intermediate catalyst species (**VIII**) regenerates the solid catalyst via elimination of the final product **4**.

Table 2
Condensation reaction of 2-aminopyridine, benzaldehyde and cyclohexylisocyanide in the presence of different loading of the catalyst under solvent-free conditions.

Entry	Catalyst	Catalyst loading (g)	Temperature (°C)	Time (h)	Yield[a] (%)	Refs.
1	–	–	r.t.	2	Trace	This work
2	$FeCl_3$·nano-SiO_2	0.02	r.t.	2	40	This work
3	$FeCl_3$·nano-SiO_2	0.02	35	1.5	80	This work
4	$FeCl_3$·Al_2O_3	0.02	35	1.5	94	This work
5	KF·γAl_2O_3	0.02	35	1.5	35	This work
6	NH_4OAc·Al_2O_3	0.05	35	2	30	This work
7	Clay	0.05	Microwave	3	86	[17]
8	Cellulose sulfuric acid	0.05	r.t.	2	94	[18]
9	$ZnCl_2$	5[b]	Microwave	1	78	[20]
10	γ-Fe_2O_3@SiO_2-OSO_3H	1[b]	35	1	92	[26]
11	nano-$LaMnO_3$	0.002	*r.t*	2	60	This work
12	**nano-$LaMnO_3$**	**0.0005**	**35**	**1.5**	**96**	This work
13	nano-$LaMnO_3$	0.001	35	1.5	96	This work
14	nano-$LaMnO_3$	0.002	35	1.5	96	This work
15	nano-$LaMnO_3$	0.005	35	1.5	95	This work
16	nano-$LaMnO_3$	0.01	35	1.5	95	This work
17	nano-$LaMnO_3$	0.02	35	1.5	95	This work

Conditions: 2-aminopyridine 1 mmol, benzaldehyde 1 mmol cyclohexylisocyanide 1 mmol.
[a] Isolated yield.
[b] mol%.

Table 3
Synthesis of various 3-aminoimidazo[1,2-*a*]pyridines in the presence of nano-$LaMnO_3$.

Entry	X	R	Product	Yield* (%)	*mp* (°C)	TON	TOF (h^{-1})
1	H	Ph	**4a**	96	178–180 (174–175) [17]	2790	372
2	H	4-Me-C_6H_4	**4b**	95	160–161 (166–169) [25]	2902	387
3	H	4-Cl-C_6H_4	**4c**	99	185–187 (179–181) [24]	3210	428
4	H	4-NMe_2-C_6H_4	**4d**	94	182–183	3138	418
5	H	2-Fluorenyl	**4e**	95	172–174	3608	481
6	H	4-OMe-C_6H_4	**4f**	91	154 (154) [52]	2822	376
7	H	4-Br-C_6H_4	**4g**	99	176–178	3654	487
8	H	2-Thiophen	**4h**	97	160–161 (168–170) [53]	2884	384
9	Me	Ph	**4i**	95	170–172	2904	387
10	Me	4-Me-C_6H_4	**4j**	94	191–192 (dec)	3002	400
11	Me	2,4-Me_2-C_6H_3	**4k**	91	198–199	3036	405
12	Me	4-Cl-C_6H_4	**4l**	98	208–209	3326	443
13	Me	4-NMe_2-C_6H_4	**4m**	94	200–202 (dec)	3278	437
14	Me	2-Fluorenyl	**4n**	94	200–201	3696	492
15	Me	4-Br-C_6H_4	**4o**	99	204–206	3794	506

Conditions: aminopyridines (1 mmol), benzaldehydes (1 mmol), cyclohexylisocyanide (1 mmol) and 0.2 mol% nano-$LaMnO_3$ (0.0005 g), stirring at 35 °C, 90 min.
* Isolated yield.

4. Conclusions

In summary, nanoparticles of perovskite type $LaMnO_3$ were prepared using sol–gel method in the presence of citric acid as a chelating agent. The XRD, TEM, SEM and EDX reveal that the $LaMnO_3$ nanoparticles prepared by calcinating the gel precursor at 650 °C have good crystallinity in perovskite phase structure. According to electron microscopic images, the nanoparticles exhibit regular morphology with homogeneous particle size distribution.

In addition, in the present study we developed a green method for synthesis the imidazo[1,2-*a*]pyridine derivatives by perovskite-type oxide $LaMnO_3$ nanoparticles as thermally stable, non-volatile, efficient recyclable heterogeneous catalyst under solvent-free condition. The advantages of this procedure over earlier reported processes include excellent yield, short reaction time, and mild condition, very low loading of catalyst and high performance of catalyst even after five runs.

Appendix A. Supplementary data

Supplementary data associated with this article can be found, in the online version, at http://dx.doi.org/10.1016/j.apcata.2013.10.026.

References

[1] A. Monge, J.A. Palop, J.C.D. Castillo, J.M. Caldero, J. Roca, G. Romero, J.D. Rio, B. Lasheras, J. Med. Chem. 36 (1993) 2745–2750.
[2] K. Toshima, R. Takano, T. Ozawa, S. Matsumara, Chem. Commun. 3 (2002) 212–213.
[3] B. Dowlati, D. Nematollahi, M.R. Othman, Int. J. Electrochem. Sci. 7 (2012) 5990–5996.
[4] Y.B. Kim, Y.H. Kim, J.Y. Park, S.K. Kim, Bioorg. Med. Chem. Lett. 14 (2004) 541–544.
[5] C. Desai, N.R. Pandya, M.M. Rajpara, K.V. Joshi, V.V. Vaghani, H.M. Satodiya, Med. Chem. Res. 21 (2012) 4437–4446.
[6] D. Elleder, T.J. Baiga, R.L. Russell, J.A. Naughton, S.H. Hughes, J.P. Noel, J.A.T. Young, Virol. J. 9 (2012) 305–311.
[7] N. Dahan-Farkas, C. Langley, A.L. Rousseau, D.B. Yadav, H. Davids, C.B. de Koning, Eur. J. Med. Chem. 46 (2011) 4573–4583.
[8] K.C. Rupert, J.R. Henry, J.H. Dodd, S.A. Wadsworth, D.E. Cavender, G.C. Olini, B. Fahmy, J. Siekierka, J. Bioorg, Med. Chem. Lett. 13 (2003) 347–350.
[9] C. Hamdouchi, B. Zhong, J. Mendoza, E. Collins, C. Jaramillo, J.E. De Diego, D. Robertson, C.D. Spencer, B.D. Anderson, S.A. Watkins, F. Zhanga, H.B. Brooks, Bioorg. Med. Chem. Lett. 15 (2005) 1943–1947.
[10] S.C. Goodacre, L.J. Street, D.J. Hallett, J.M. Crawforth, S. Kelly, A.P. Owens, W.P. Blackaby, R.T. Lewis, J. Stanley, A.J. Smith, P. Ferris, B. Sohal, S.M. Cook, A. Pike, N. Brown, K.A. Wafford, G. Marshall, J.L. Castro, J.R. Atack, J. Med. Chem. 49 (2006) 35–38.
[11] K. Groebke, L. Weber, F. Mehlin, Synlett 6 (1998) 661–663.
[12] H. Bienayme, K. Bouzid, Angew. Chem. Int. Ed. 37 (1998) 2352–2355.
[13] C. Blackburn, B. Guan, P. Fleming, K. Shiosaki, S. Tsai, Tetrahedron Lett. 39 (1998) 3635–3638.
[14] C. Hulme, Y.S. Lee, Mol. DiversityV 12 (2008) 1–15.
[15] C. Che, J. Xiang, G.X. Wang, R. Fathi, J.M. Quan, Z. Yang, J. Comb. Chem. 9 (2007) 982–989.

[16] M.A. Mironov, M.I. Tokareva, M.N. Ivantsova, V.S. Mokruskin, Russ. Chem. Bull. Int. Ed. 55 (2006) 1835–1839.
[17] R.S. Varma, D. Kumar, Tetrahedron Lett. 40 (1999) 7665–7669.
[18] A. Shaabani, A. Maleki, J. Moghimi Rad, E. Soleimani, Chem. Pharm. Bull. 55 (2007) 957–958.
[19] A. Shaabani, E. Soleimani, A. Maleki, Monatsh. Chem. 138 (2007) 73–76.
[20] A.L. Rousseau, P. Matlaba, C.J. Parkinson, Tetrahedron Lett. 48 (2007) 4079–4082.
[21] A. Shaabani, F. Rezazadeh, E. Soleimani, Monatsh. Chem. 139 (2008) 931–933.
[22] A.T. Khan, R.S. Basha, M. Lal, Tetrahedron Lett. 53 (2012) 2211–2217.
[23] A. Shaabani, E. Soleimani, A. Maleki, Tetrahedron Lett. 47 (2006) 3031–3034.
[24] M. Adib, M. Mahdavi, M.A. Noghani, P. Mirzaei, Tetrahedron Lett. 48 (2007) 7263–7265.
[25] M. Adib, E. Sheikhi, N. Rezaei, Tetrahedron Lett. 52 (2011) 3191–3194.
[26] S. Rostamnia, K. Lamei, M. Mohammadquli, M. Sheykhan, A. Heydari, Tetrahedron Lett. 53 (2012) 5257–5260.
[27] S.M. Ireland, H. Tye, M. Whittaker, Tetrahedron Lett. 44 (2003) 4369–4371.
[28] Y. Lu, W. Zhang, QSAR Comb. Sci. (2004) 23–31.
[29] C. Blackburn, Tetrahedron Lett. 39 (1998) 5469–5472.
[30] W.R. Moser, Catalytic Chemistry of Solid State Inorganics, New York Academy of Sciences, New York, 1976.
[31] G. Centi, F. Trifiro, Catal. Rev. Sci. Eng. 28 (1986) 165–184.
[32] N. Mizuno, M. Misono, Chem. Rev. 98 (1998) 199–218.
[33] C.D. Chandler, C. Roger, M.J. Hampden-Smith, Chem. Rev. 93 (1993) 1205–1241.
[34] R. Robert, M.H. Aguirre, P. Hug, A. Reller, A. Weidenkaff, Acta Mater. 55 (2007) 4965–4972.
[35] M. Nandia, K. Sarkara, M. Seikhc, A. Bhaumik, Microporous Mesoporous Mater. 143 (2011) 392–397.
[36] H. Aono, E. Traversa, M. Sakamoto, Y. Sadaoka, Sens. Actuators, B: Chem. 94 (2003) 132–139.
[37] R. Horyn, R. Klimkiewicz, Appl. Catal., A: Gen. 370 (2009) 72–77.
[38] N. Pal, M. Paul, A. Bhaumik, Appl. Catal., A: Gen. 393 (2011) 153–160.
[39] M. Yazdanbakhsh, H. Tavakkoli, S.M. Hosseini, Desalination 281 (2011) 388–395.
[40] H. Tavakkoli, M. Yazdanbakhsh, Microporous Mesoporous Mater. 176 (2013) 86–94.
[41] A.V. Salker, N.J. Choi, J.H. Kwak, B.S. Joo, D.D. Lee, Sens. Actuators, B: Chem. 106 (2005) 461–467.
[42] S.V. Ley, M.D. Smith, C. Ramarao, A.F. Stepan, H. Tanaka, US 2005215804., U.S. Pat. Appl. Pub., 2005.
[43] M.D. Smith, A.F. Stepan, C. Ramarao, P.E. Brennan, S.V. Ley, Chem. Commun. (2003) 2652–2653.
[44] S.P. Andrews, A.F. Stepan, H. Tanaka, S.V. Ley, M.D. Smith, Adv. Synth. Catal. 347 (2005) 647–654.
[45] S. Lohmann, S.P. Andrews, B.J. Burke, M.D. Smith, J.P. Attfield, H. Tanaka, K. Kaneko, S.V. Ley, Synlett 8 (2005) 1291–1295.
[46] G. Pilania, P.X. Gao, R. Ramprasad, J. Phys. Chem. C 116 (2012) 26349–26357.
[47] J. Safaei-Ghomi, S. Zahedi, M.A. Ghasemzadeh, Iran. J. Catal. 2 (2012) 27–30.
[48] J.H. Shi, L. Zhou, L.Z. Wang, W. Yan, J. Zhejiang Univ. Tech. 34 (2006) 360–363.
[49] V. Raju, R. Radhakrishnan, S. Jaenicke, G.K. Chuah, Catal. Today 164 (2011) 139–142.
[50] T. Aoyama, S. Murata, T. Takido, M. Kodomari, Tetrahedron 63 (2007) 11933–11937.
[51] M. Kakihana, M. Arima, M. Yoshimura, N. Ikeda, Y. Sugitani, J. Alloys Compd. 283 (1999) 102–105.
[52] A. Shaabani, E. Soleimani, A. Maleki, J. Moghimi-Rad, Synth. Commun. 38 (2008) 1090–1095.
[53] A. Shahris, S. Esmati, Synlett 24 (2013) 595–602.